JCHR (2023) 13(2), 379-390

Journal of Chemical Health Risks

www.jchr.org

ORIGINAL ARTICLE

Adsorptive Removal of Noxious Nickel Ions from Aqueous Mediums Using Titanium Dioxide Nanoparticles: A Comparative Assessment with an Eco-friendly Adsorbent as Well as Isotherm and Kinetic Modeling

Elnaz Rezaei-Aghdam, Ali Shamel*, Mohammad Khodadadi-Moghaddam, Gholamreza Ebrahimzadeh-Rajaei*, Sahar Mohajeri

Department of Chemistry, Ardabil Branch, Islamic Azad University, Ardabil, Iran

(Received: 10 May 2021 Accepted: 17 January 2022)

KEYWORDS

Toxic heavy metal;
Adsorption;
Nickel ions;
TiO_2 nanoparticles;
Kinetics;
Isotherms

ABSTRACT: In the present study, natural and synthetic adsorbents were used to remove nickel ions through the adsorption process. First, TiO_2 nanoparticles (NPs) were prepared through the sol-gel method. The synthesized samples were then characterized using X-ray diffraction spectroscopy (XRD), Fourier transform-infrared (FTIR) spectroscopy, scanning electron microscopy (SEM), transmission electron microscopy (TEM), and N_2 adsorption/desorption isotherms (BET). The influences of different operational parameters including adsorbate content, pH, adsorbent concentration, contact time, ionic strength, and stirring speed were also explored. According to the results, the pseudo-second-order kinetic model showed the best performance in evaluating the experimental data when using both adsorbents. The adsorption of nickel cations by the thin film membrane on the surface of TiO_2 NPs is a rate-determining step of the removal reaction. The removal rate constants of nickel ions from aqueous solutions by TiO_2 NPs and pomegranate peel were evaluated to be 0.013 and 0.018 g mg^{-1} min^{-1}, respectively. The thermodynamic parameters such as Gibbs free energy, enthalpy, and entropy were also determined. Nickel removal processes in all cases were endothermic and spontaneous. The removal mechanism also followed physical adsorption. Equilibrium data were fitted with Langmuir, Freundlich, Temkin, and Dubinin–Radushkevich models. The results showed that the adsorption of Ni^{2+} on TiO_2 NPs and pomegranate peel followed Freundlich and Temkin isothermal models, respectively. Based on the calculated removal percentage, TiO_2 is a better adsorbent for removing Ni^{2+} from the aqueous medium as compared to pomegranate peel.

INTRODUCTION

Regarding the increasing release of heavy metals into the environment through industrial and natural processes, the process of heavy metal removal has become one of the most important concerns [1-6]. Accumulation of metallic cations in the tissues of living creatures can lead to various physiological disorders [7-9]. Nickel is one of the toxic and non-biodegradable heavy metals which can be found in wastewater [10, 11]. Industrial procedures such as mining, galvanization, coloring, batteries fabrication, and melting are among the major sources of Ni release [12, 13]. Trace levels of nickel are necessary for activating some enzymes in the body, but its high levels (above the permitted limit) in water resources can lead to various diseases such as lung cancer, renal and skin inflammation as well as gastric disorders [14-16]. Heavy metal-induced damages can be prevented by avoiding their release into the environment including the water sources [17-

---

*Corresponding authors: a_shamel@iauardabil.ac.ir; gh_rajaei@iauardabil.ac.ir (A. Shamel & Gh. Ebrahimzadeh-Rajaei)

DOI: 10.22034/jchr.2022.1930233.1306

19]. Various approaches have been employed for removal and separation of the heavy metals from water resources among which, chemical and electrochemical decomposition, membrane and biologic processes, ionic exchange, and physical procedures such as reverse osmotic electrodialysis, solvent evaporation and extraction, and surface adsorption can be mentioned [20-22]. Some of these methods suffer from several drawbacks such as low efficiency, waste generation and high costs due to additional environmental problems. Among the mentioned methods, surface adsorption has found remarkable popularity due to its feasibility and improved cost-effectiveness [23-25].

Regarding the significance of the treatment and recovery of the heavy metal-contaminated water resources, huge attempts have been devoted to developing efficient and inexpensive adsorbents with high surface area, porosity, and surface functional groups from the agricultural wastes [26-28]. Metal oxide NPs such as ferrite oxide, manganese oxide, aluminum oxide, and titanium oxide have been recently applied for heavy metal removal from the aqueous media. These metal oxides are more cost-effective and biocompatible compared to the other conventional adsorbents [29-31].

Titanium dioxide (TiO_2) has found extensive scientific significance, due to its promising characteristics such as non-toxicity, high-temperature stability, and excellent stability under ultraviolet radiation [32-34]. Under UV radiation, TiO_2 can exhibit photocatalytic activities [35, 36]. The behavior of TiO_2 is highly dependent on its crystallographic structure, shape, and particle size [37, 38]. This metal oxide has been widely employed in various applications such as pigments, coatings, adhesives, papers, paperboards, plastics, rubbers, printing inks, textiles, catalysis systems, ceramics, pavements and coating materials, cosmetics, pharmaceuticals, water purifying agents, edible colors, and automobile industry [39].

Pomegranate is one of the native fruits of Iran. Iran has the first rank in pomegranate production (more than one million tons per year). Pomegranate peel is one of the main wastes of pomegranate processing factories. Its low price and high technological and biological value have fueled a huge deal of studies. Pomegranate peel can be used as a low-cost, non-toxic, natural, reusable, high-capacity, efficient, and eco-friendly adsorbent for the removal of toxic pigments and heavy metals [40].

This research is thus aimed to remove Ni^{2+} from aqueous media using TiO_2 and pomegranate peel adsorbents. Parameters such as contact time, pH, adsorbent concentration, ionic strength, adsorbate content were optimized. Exploring the best kinetic models and isotherms is also among the objectives of this study.

MATERIALS AND METHODS

Materials and equipment

Nickel (II) nitrate ($Ni(NO_3)_2 \cdot 6H_2O$, Merck, 99%), Titanium (IV) chloride ($TiCl_4$, Merck, 99%), ethanol (C_2H_5OH, Merck, 99.9%), hydrochloric acid (HCl, Chongqing Dongchuan Chemical Company, 36%), sodium hydroxide (NaOH, Tianjin Yongda chemical reagent Company, 96%), sodium chloride (NaCl, Merck, extra pure), and pomegranate peel powder were used in this research. Double-distilled water was also used as the solvent.

This study also involved using pH-meter (781 pH/Ion Meter manufactured by Metrohm, Herisau Switzerland), ultrasonic bath (Ultrasonic-cleaner XPS 120-3L), shaker (Compact Shaker KS 15), laboratory oven (KSL-1700X-G) , atomic absorption spectroscopy (Pekin Elmer, AANALYST 300), and FTIR spectrophotometer (Perkin Elmer Spectrum ASLII PEDS 1.60).

Synthesis of TiO_2 nanoparticles

TiO_2 NPs were synthesized through a solution-based sol-gel method [41, 42]. Typically, 15 mL titanium tetrachloride was mixed with 60 mL anhydrous ethanol within a 250-mL flask under vigorous stirring. Two drops of concentrated HCl were added to the mixture. The solution was sonicated for 75 min at 25 °C and allowed to rest for one week at ambient temperature for complete gelation. The resulting gel was dried in an oven at 120 °C and then calcined for 6 h at 350 °C. After cooling, the black fine powders were collected as titanium dioxide NPs.

Adsorption experiments

Various operational variables including contact time, pH, adsorbent dose, ionic strength, Ni concentration, and stirring rate were optimized to enhance the adsorption efficiency. The standard solutions of Ni^{2+} were prepared with different concentrations (10, 20, 30, 40, and 50 mg L^{-1}) whose absorbance was measured by an atomic absorption spectrophotometer. Then, the standard curve was constructed for determining the residual concentration of nickel ions.

The effect of ionic strength was investigated. For this purpose, 1000 mL of Ni^{2+} solution (100 mg L^{-1}) was provided by dissolving $Ni(NO_3)_2.6H_2O$ in distilled water, while the solution pH was adjusted at 9. Regarding the cationic nature of Ni^{2+} solution, its adsorption process requires an alkaline medium. The solutions with various ionic strengths (0.01, 0.02. 0.03. 0.04. 0.05. 0.06, and 0.07 mol L^{-1}) were prepared using NaCl solution. 0.02 g of adsorbent was then added to each solution and stirred up to 140 rpm using a magnetic stirrer. Afterward, the solutions were filtered and centrifuged. The residual concentrations of the solutions were measured by an atomic absorption spectrophotometer.

The ionic strength (I) can be determined by the following equation [43]:

$$I = \frac{1}{2}\sum C_i Z_i^2 \qquad (1)$$

in which C_i shows the ion concentration [44], while Z_i is the ionic charge of the electrolyte [44, 45]. The following equation can be used to assess the removal percentage of nickel ions [45]:

$$R(\%) = ((C_0 - C_e)/C_0) \times 100 \qquad (2)$$

where q_e and q_t are expressed as:

$$q_e = \frac{(C_0 - C_e) \times V}{W} \qquad (3)$$

$$q_t = \frac{(C_0 - C_t) \times V}{W} \qquad (4)$$

in which, C_e (mg L^{-1}) shows the equilibrium concentration of the adsorbate. C_0 and C_t (mg L^{-1}) are the initial and moment concentration of the adsorbate in the liquid phase, respectively. q_e and q_t (mg g^{-1}) represent the adsorbate content in the equilibrium and an arbitrary time of t, respectively. V(L) represents the solution volume, while the adsorbent amount is shown by W (g).

Adsorption kinetics

5 mL of Ni^{2+} solution (100 mg L^{-1}, and pH=9) was provided. Then, 0.02 g of each adsorbent was added into the flask followed by stirring at 200 rpm for 1-90 min. After specific intervals, the solution was filtered and centrifuged. The final residual concentrations of each solution were measured using an atomic absorption spectrophotometer.

Effects of temperature

To explore the effects of temperature, 0.02 g of each adsorbent was added to 25 mL of Ni^{2+} solution (100 mg L^{-1}, pH=9) followed by stirring at 200 rpm at various temperatures of 25, 35, 45, and 55 ˚C. The solutions were then filtered and centrifuged and their final residual concentrations were measured by an atomic absorption spectrophotometer.

Isotherm experiments

25 mL of Ni^{2+} solution was prepared at different concentrations of 25, 50, 75, 100, 125, and 150 mg L^{-1} and pH of 9. To determine the thermodynamic parameters, an optimized amount (0.02 g) of adsorbent was added to the solutions which were stirred at 200 rpm at 25, 35, 45, and 55˚C. Afterward, the solutions were filtered and centrifuged to measure the residual concentration of the samples using an atomic absorption spectrophotometer.

RESULTS AND DISCUSSION

Characterization of adsorbents

The XRD pattern of TiO_2 NPs is depicted in Figure 1. The peaks at 2Θ = 25.41˚, 37.97˚, 48.11˚, 54.01˚, 55.18˚, 62.85˚, 70.47˚, and 75.41˚ correspond to (101), (004), (200), (105), (211), (204), (220), and (215) planes, respectively, indicating the formation of TiO_2 NPs whit a tetragonal crystalline structure (JCPDS No.21-1272) [46].

The Scherrer equation can be expressed by:

$$D = (K \times \lambda)/(\beta \times \cos\theta) \qquad (5)$$

where D shows the mean crystalline size, *K* denotes a dimensionless shape factor (~0.9); λ represents the X-ray wavelength (0.15406 nm); β is the full width at half maximum intensity (FWHM), and θ stands for the Bragg angle [47]. The mean size of TiO_2 NPs was approximately 12.08 nm.

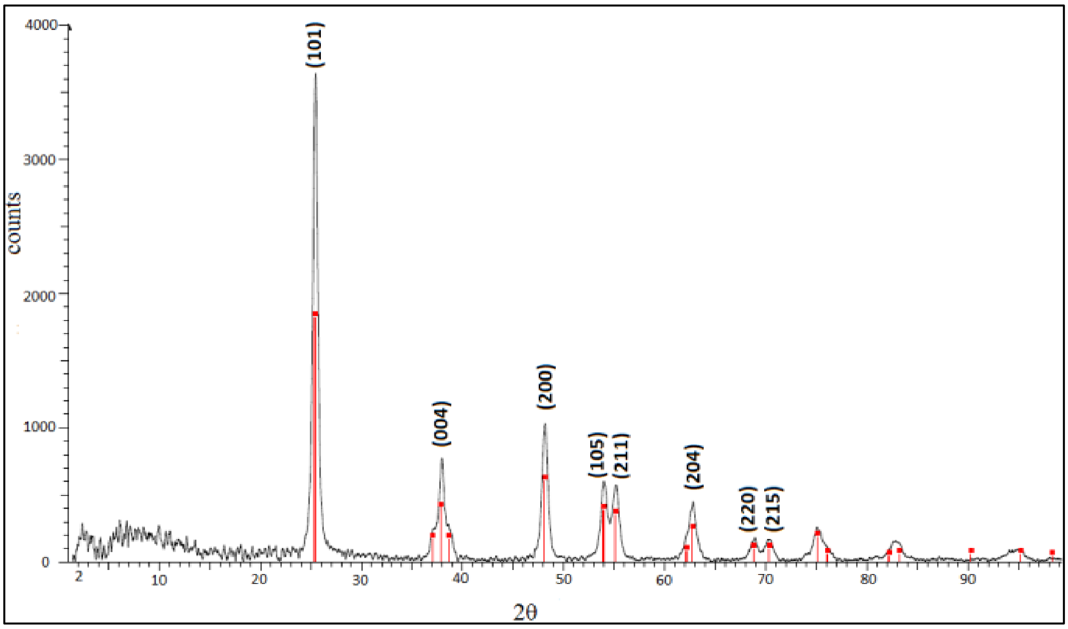

Figure 1. XRD pattern of TiO_2 nanoparticles synthesized by sol-gel method

The functional groups of the samples can be determined by FTIR spectroscopy. According to Figure 2a, the peaks at 3200-3500 cm^{-1} indicate the stretching vibrations of O-H bonds in ethanol. The peaks appearing at 400-500 cm^{-1} could be ascribed to the stretching vibrations of Ti-O [48]. FTIR spectra of the pomegranate peel can be found in Figure 2b where the peaks at 1000-1500 cm^{-1} show the presence of lignin. The broad band at 1500-2000 cm^{-1} indicates the existence of carboxyl groups and proteins, whereas those appearing in the range of 2000-2500 cm^{-1} can be attributed to the ester compounds. The C═C stretching band of the alkyne group was detected at 2854-2924 cm^{-1}. The broad peaks at 3000-3500 cm^{-1} also correspond to polysaccharides and water [39].

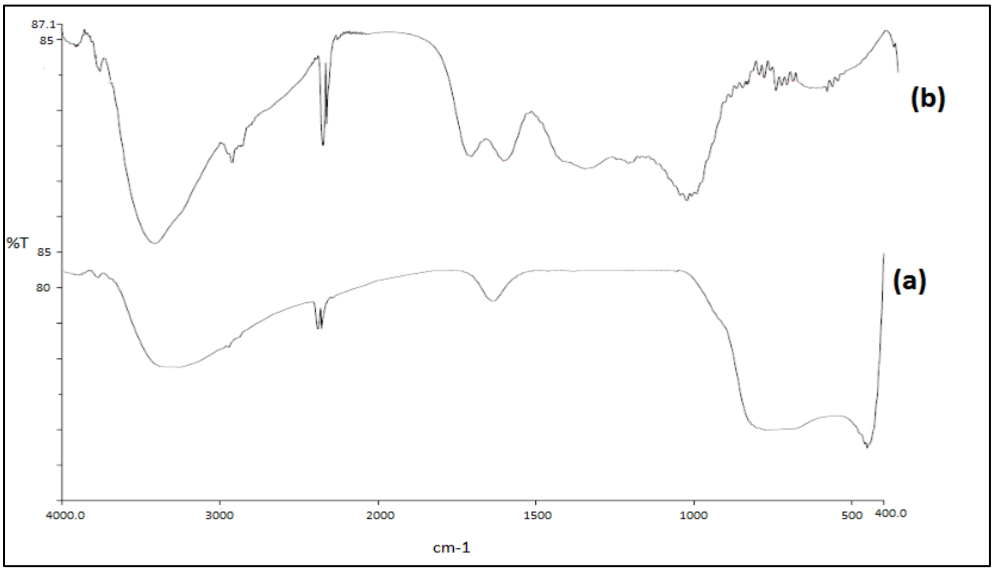

Figure 2. FTIR spectra of (a) TiO_2 NPs synthesized by sol-gel method, and (b) pomegranate peel

Figure 3a depicts the hollow structure of synthesized NPs with an average nanoparticle size of 22.32 nm, confirming the successful synthesis of nanoparticles. Also, TEM results (Figure 3b) show the formation of the small spherical nanoparticles.

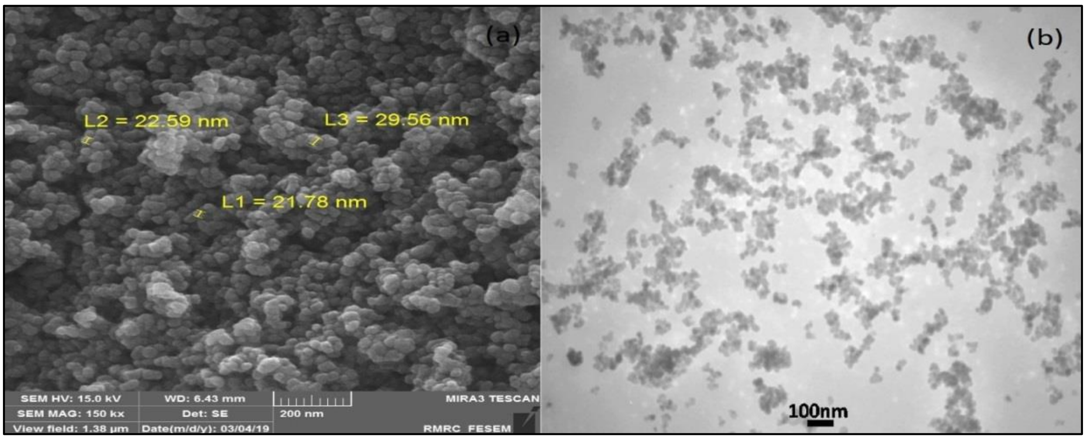

Figure 3. a) SEM and b) TEM images of TiO_2 NPs synthesized by sol-gel method

BET results of titanium dioxide nanoparticles showed that the specific surface area, pore volume, and pore size were 50.12 m^2 g^{-1}, 0.1746 cm^3 g^{-1}, and 1.22 nm, respectively.

Operational parameters

The initial concentration of Ni^{2+} ions, pH of solutions, and stirring rate were the three main operational parameters that were explored in this study. The optimal nickel ion removal from aqueous media involved the initial concentration of 100 mg L^{-1}, solution pH of 9, and stirring rate of 200 rpm. In the case of TiO_2 NPs, 0.02 g of adsorbent was employed for the contact time of 5 min. For pomegranate peel, the adsorbent dose and contact time were determined at 0.02 g, and 7 min, respectively.

Figure 4 shows the residual concentration of Ni^{2+} ions versus ionic strength. As can be seen, the residual concentration increased by incrementing the ionic strength of both adsorbents; reflecting the high Ni^{2+} adsorption ability of both adsorbents at lower ionic strengths. The optimal ionic strength was near zero.

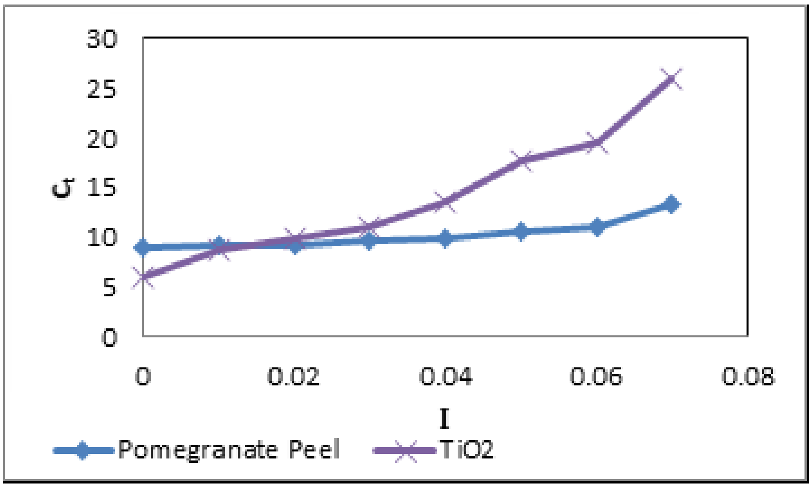

Figure 4. The effect of ionic strength on the Ni^{2+} adsorption by TiO_2 NPs and pomegranate peel

Kinetic and mechanism investigations

According to the pseudo-first-order kinetic model, diffusion occurs inside a layer depending on the solid capacity. Under such conditions, the temporal variations of the adsorption are directly related to the abundance of unoccupied active sites on the adsorbent. For the pseudo-second-order model, however, the chemisorption is in decelerating stage and controls the adsorption processes. This model relies on the solid phase adsorption in which the occupation rate of the adsorption sites is directly correlated with the square of the number of unoccupied sites [49, 50]. The general forms of the first- and second-order kinetic models can be expressed by:

$$\ln(q_e - q_t) = \ln q_e - k_1 \cdot t \qquad (6)$$

$$\left(\frac{t}{q_t}\right) = \left(\frac{1}{k_2 \cdot q_e^2}\right) + \left(\frac{1}{q_e}\right) \cdot t \qquad (7)$$

in which q_e and q_t (mg g^{-1}) show the amounts of adsorbate at equilibrium and the arbitrary time of t, respectively. k_1 (min^{-1}) and k_2 (g mg^{-1} min^{-1}) also respectively indicate the first- and second-order equilibrium kinetic constants. The correlation coefficient parameter can be determined after plotting the related diagrams for each model.

Table 1 presents the pseudo-first-order and pseudo-second-order kinetic models. Accordingly, the pseudo-second-order kinetic model offered a better correlation coefficient, indicating its ability to describe the kinetics of Ni^{2+} adsorption by both adsorbents. For comparison, the data reported by Xiaotao Zhang et al. for the removal of Ni (II) ions on the lignocellulose/montmorillonite (LNC/MMT) nanocomposite are also presented in Table 1 [51]. Comparison of q_e results showed that both adsorbents used in this study are suitable for the removal of Ni (II) ions.

Figure 5 shows the Ni^{2+} removal percentage for pomegranate peel and TiO_2 NPs. As can be seen, TiO_2 NPs exhibited a higher removal percentage compared to pomegranate peel.

Table 1. The kinetic parameters from the pseudo-first-order and pseudo-second-order kinetic models for Ni^{2+} adsorption on TiO_2 nanoparticles and pomegranate peel.

	Pseudo-first-order kinetic model			**Pseudo-second-order kinetic model**		
Samples	**k_1(min^{-1})**	**q_e (mg g^{-1})**	**R^2**	**k_2 (g $mg^{-1}min^{-1}$)**	**q_e (mg g^{-1})**	**R^2**
Pomegranate peel	9×10^{-5}	2.71	0.2701	0.018	107.52	0.9993
TiO_2	0.0002	2.71	0.8485	0.013	108.69	0.9960
LNC/MMT	0.0256	41.79	0.7254	0.004	87.72	0.9980 [51]

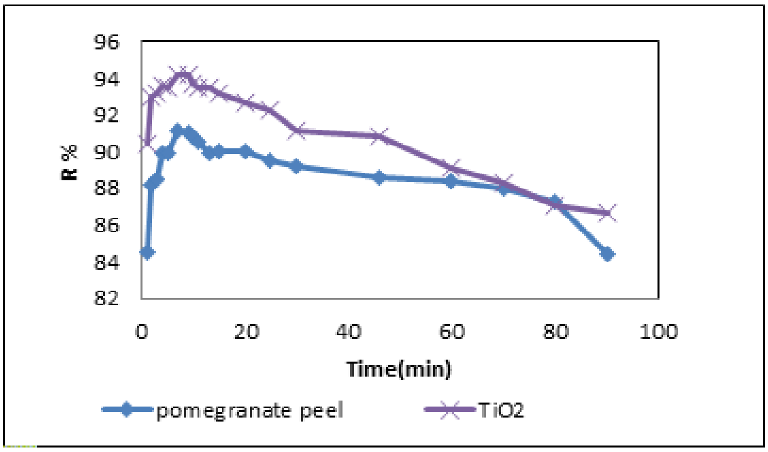

Figure 5. Ni^{2+} removal percentage versus time for the TiO_2 NPs and pomegranate peel

According to by Pung et al. [52], nanoparticles eliminate heavy metal ions through two types of mechanisms: (i) physical adsorption, and (ii) reduction/oxidation by photo-generated electron-hole pairs. Based on the results of this study, the removal mechanism of nickel ions by TiO_2 NPs is based on physical adsorption. As measured by the zeta potential analyzer, TiO_2 NPs are positively charged (56.0 mV) as shown in Figure 6. Following the addition of NaOH, the TiO_2 NPs got negative surface charges mainly contributed by the OH^- groups. These OH^- groups then served as active adsorption sites for the elimination of Ni^{2+} metal ions into the solution. Cationic nickel in the aqueous solution tended to react with hydroxide groups to form a thin film on the surface of TiO_2 nanoparticles [52]. So, the adsorption of nickel cations by the thin film membrane created on the surface of TiO_2 NPs is a rate-determining step of the removal reaction.

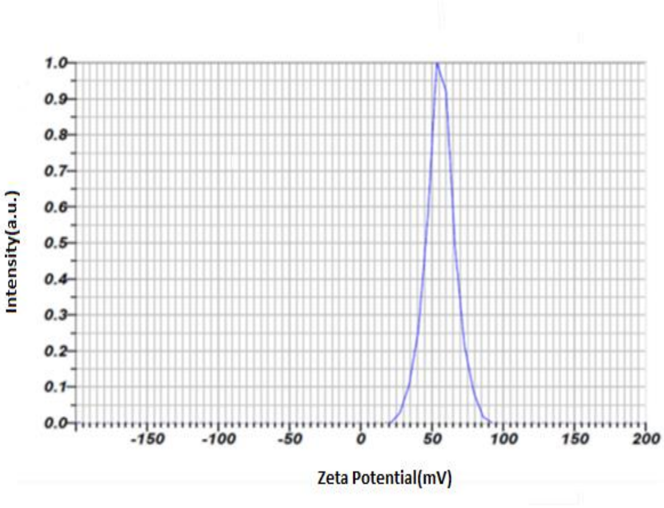

Figure 6. Surface charge of TiO_2 nanoparticles measured by zeta potential.

Thermodynamic studies

Thermodynamic studies can be used to theoretically predict the modality of chemical reaction under specific conditions. Thermodynamic indices including Gibbs free energy, enthalpy, and entropy were calculated by the following equations [53]:

$$K_C = \frac{C_S}{C_e} \tag{8}$$

$$\Delta G° = -RT \ln K_C \tag{9}$$

$$\ln K_C = \left(\frac{\Delta S°}{R}\right) - \left(\frac{\Delta H°}{RT}\right) \tag{10}$$

In the above equations, K_c shows the adsorption equilibrium constant; while C_s and C_e (mg dm^{-3}) denotes the equilibrium adsorbate content on the adsorbent surface and in the solution phase, respectively. T (K) indicates the solution temperature, and R (J mol^{-1} K^{-1}) represents the universal gas constant. The calculated thermodynamic parameters are sumerized in Table 2.

Table 2. Thermodynamic parameters of Ni^{2+} adsorption onto the surface of TiO_2 NPs and pomegranate peel

Samples	**T**	**C_e**	**C_s**	**K_c**	**ΔG°**	**ΔS°**	**ΔH°**
	(K)	**(mg dm^{-3})**	**(mg dm^{-3})**		**(kJ $mole^{-1}$)**	**(kJ mole K^{-1})**	**(kJ $mole^{-1}$)**
Pomegranate peel	298.15	8.90	91.09	10.23	-5.76	0.23	64.83
	308.15	4.60	95.39	20.69	-7.76		
	318.15	3.10	96.89	31.15	-9.09		
	328.15	0.76	99.23	129.35	-13.26		
TiO_2	298.15	9.98	90.01	9.01	-5.45	0.34	98.26
	308.15	3.91	96.08	24.52	-8.19		
	318.15	1.64	98.35	59.83	-10.82		
	328.15	0.26	99.73	383.21	-16.22		

Based on Table 2, the Ni^{2+} adsorption onto the surface of TiO_2 NPs and pomegranate peel is an endothermic and spontaneous process.

Isotherms of adsorption

In this study, four main isotherm models were considered. The Langmuir model involves adsorption at some homogenous sites inside the adsorbent. In the Freundlich isotherm, heterogeneous surfaces with non-uniform adsorption heat distributions are responsible for the adsorption. Based on the Temkin model, the adsorption heat of all molecules is linearly declined in the layer due to the adsorbent-adsorbate interactions. The Radushkevich model states that the adsorbent surface is not homogenous and the adsorption potential of the adsorbent surface is not uniform. The linear forms of these equations can be expressed as [54]:

$$\frac{C_e}{q_e} = \left(\frac{1}{K_L Q_m}\right) + \frac{C_e}{Q_m} \qquad (11)$$

$$\log q_e = \log K_F + \left(\frac{1}{n}\right) \log C_e \qquad (12)$$

$$q_e = B_T \ln A_T + B_T ln C_e \qquad (13)$$

$$\ln q_e = \ln q_m - K_D \varepsilon^2 \qquad (14)$$

in which, q_e is the equilibrium amount of adsorbate, C_e shows the equilibrium concentration of the solution, K_L denotes the equilibrium constant, and Q_m shows the maximum adsorption capacity. K_f is the adsorption capacity per concentration unit, and 1/n represents the isotherm type. A_T is Temkin constant, and B_T is related to the heat of adsorption. ε represents the plan potential and K_D indicates the Dubinin- Radushkevich isotherm constant.

Only the curves obtained from the assessment of Freundlich and Temkin models are represented in Figure. 7. Table 3 lists the isothermal parameters for Ni^{2+} adsorption onto the surface of TiO_2 NPs and pomegranate peel. As can be seen, Ni^{2+} adsorption onto the surface of TiO_2 NPs followed the Freundlich isotherm; while Temkin isotherm managed to properly describe the adsorption process of Ni^{2+} onto the pomegranate peel. For comparison purposes, the data reported by Rajvinder Kaur et al. are also reported in Table 3. They used agricultural residues as an adsorbent to remove Ni(II) ions [55]. Due to the high q_m values, it can be concluded that the adsorbents used in this work are suitable to remove Ni(II) ions.

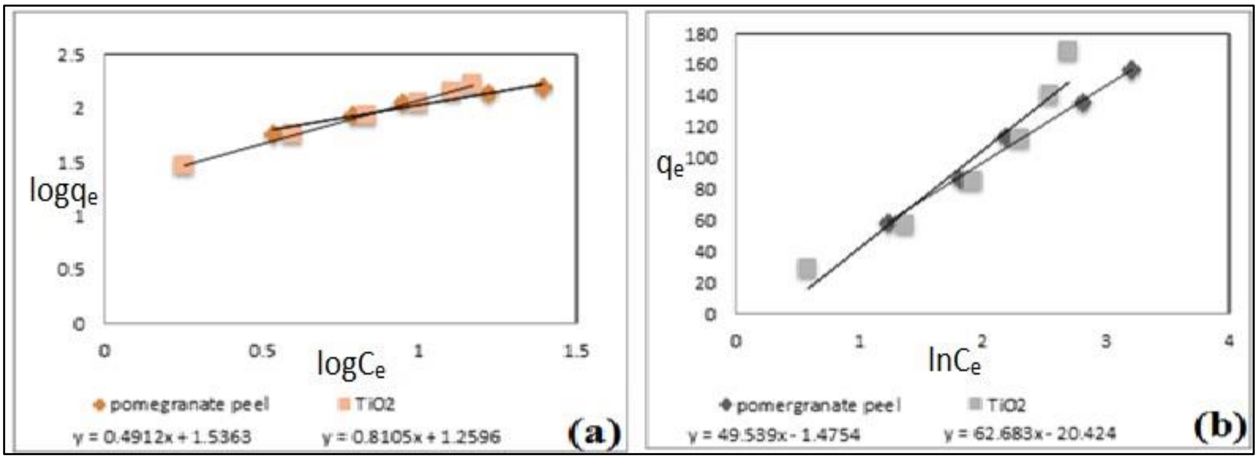

Figure 7. Isotherms of Ni^{2+} adsorption onto the surface of TiO_2 NPs and pomegranate peel a) Freundlich and b) Temkin isotherms

Table 3. Isothermal parameters for Ni^{2+} adsorption onto the surface of TiO_2 NPs and pomegranate peel

Samples	**Langmuir Isotherm**			**Freundlich Isotherm**			
	Q_m (mg g^{-1})	**K_L(L mg^{-1})**	**R^2**	**1/n**	**n**	**K_F**	**R^2**
Pomegranate peel	188.67	0.16	0. 9710	0.49	2.03	34.37	0.9591
TiO_2	454.54	0.03	0.8556	0.81	1.23	18.18	0.9974
Agricultural residues	15.60	0.06	0.9800	0.46	2.14	0.66	0.9100 [55]

Samples	**Temkin Isotherm**			**Dobinin-Radoskovich Isotherm**		
	A_T (L mg^{-1})	**B_T**	**R^2**	**q_m**	**K_D (mol^2 $kJ^{2\ -1}$)**	**R^2**
Pomegranate peel	0.97	49.53	0.9893	108.44	3×10^{-7}	0.7341
TiO_2	1.01×10^{13}	0.0148	0.9256	123.92	1×10^{-6}	0.8363
Agricultural residues	0.52	686.86	0.9600	14.20	1.8×10^{-3}	0.9800 [55]

CONCLUSIONS

In this research, the removal of Ni^{2+} from aqueous solutions was investigated using TiO_2 nanoparticles and pomegranate peel. Initially, the selected adsorbents were prepared through the sol-gel method. Then synthesized materials were successfully characterized using XRD, SEM, TEM, BET, and FTIR techniques. Moreover, the effects of some operational variables such as pH, adsorbent dosage, initial concentration, stirring rate, and temperature were assessed. The best results can be achieved for nickel content of 100 mg L^{-1}, pH of 9, and stirring rate of 200 rpm. In the case of TiO_2 NPs, the adsorbent dose of 0.02 g at a contact time of 5 min and near-zero ionic strength led to the best outcomes; while for pomegranate peel, the optimal adsorption efficiency was achieved when 0.02 g pomegranate peel was used for 7 min at an ionic strength of zero. Various kinetic models were analyzed under optimal conditions. The pseudo-second-order kinetic model exhibited the best performance in describing Ni^{2+} adsorption by both adsorbents. The removal mechanism was physisorption. In terms of removal percentage, TiO_2 NPs outperformed pomegranate peel. Thermodynamic studies also revealed that Ni^{2+} adsorption onto the surface of TiO_2 NPs and pomegranate peel is endothermic and spontaneous. According to the correlation coefficients (R^2), the Temkin model was best isothermal model in describing Ni^{2+} adsorption on pomegranate peel; while the Freundlich model properly described the adsorption process by TiO_2 NPs.

ACKNOWLEDGEMENTS

This article was derived from PhD degree thesis in the Islamic Azad University-Ardabil branch.

Conflict of interest

Authors have no conflicts of interest to disclose.

Funding

This research did not receive any specific grant from funding agencies in the public, commercial, or not-for-profit sectors.

Authors' contributions

All authors contributed to data analysis, drafting, and revising the paper and are responsible for all the aspects of this work.

REFERENCES

1. Darmokoesoemo H., Kuncoro E. P., Supriyanto G., Manuharab Y.S.W., 2020. Models, kinetics, and thermodynamics for the adsorption of Pb^{2+} and Cd^{2+} metal ions by solid tofu waste immobilized on silica's SURFAC. Moroccan Journal of Chemistry. 8(1), 2012-2023.
2. Fekri R., Mirbagheri S.A., Fataei E., Ebrahimzadeh-Rajaei G., Taghavi L., 2021. Organic compound removal from textile wastewater by photocatalytic and sonocatalytic processes in the presence of copper oxide nanoparticles. Anthropogenic Pollution. 5(2), 93-103.
3. Hosseini M., Nabavi S.M.B., Nabavi S.N., Pour N.A., 2015. Heavy metals (Cd, Co, Cu, Ni, Pb, Fe, and Hg) content in four fish commonly consumed in Iran: risk assessment for the consumers. Environmental monitoring and assessment. 187(5), 1-7.
4. Iqhrammullah M., Hedwig R., Karnadi I., Kurniawan K., Olaiya N., Mohamad Haafiz M., Abdul Khalil H., Abdulmadjid S., 2020. Filler-Modified Castor oil-based polyurethane foam for the removal of aqueous heavy metals detected using laser-induced breakdown spectroscopy (LIBS) technique. Polymers. 12(4), 903.
5. Li X., Zhang L., 2019. Removing Pb^{2+} by Adsorption over Thiol-Functionalized Mesoporous Silica. Russian Journal of Physical Chemistry A. 93(9), 1804-1808.
6. Poorsadeghi S., Kassaee M., Fakhri H., Mirabedini M., 2017. Removal of arsenic from water using aluminum nanoparticles synthesized through arc discharge method. Iranian Journal of Chemistry and Chemical Engineering (IJCCE). 36(4), 91-99.
7. Ebrahimzadeh Rajaei G., Aghaie H., Zare K., Aghaie M., 2012. Adsorption of Ni (II) and Cd (II) ions from aqueous solutions by modified surface of Typha latifolia L. root, as an economical adsorbent. Journal of Physical & Theoretical Chemistry. 9(3), 137-147.
8. Lucio M., Barbir R., Lovrenčić M. V., Varžić S. C., Ljubić S., Duvnjak L. S., Šerić V., Milić M., Lovaković B. T., Krivohlavek A., 2020. Association between arsenic exposure and biomarkers of type 2 diabetes mellitus in a Croatian population: A comparative observational pilot study, Science of The Total Environment. 720, 137575.
9. Srivastava V., Weng C., Singh V., Sharma Y., 2011. Adsorption of nickel ions from aqueous solutions by nano alumina: kinetic, mass transfer, and equilibrium studies. Journal of Chemical & Engineering Data. 56(4), 1414-1422.

10. Parmar M., Thakur L.S., 2013. Heavy metal Cu, Ni and Zn: toxicity, health hazards and their removal techniques by low cost adsorbents: a short overview. International Journal of Plant, Animal and Environmental Sciences. 3(3), 143-157.

11. Tran L.T., Tran H.V., Le T.D., Bach G.L., Tran L.D., 2019. Studying Ni (II) adsorption of magnetite/graphene oxide/chitosan nanocomposite. Advances in Polymer Technology. 2019, 8124351.

12. Khan F.S.A., Mubarak N.M., Tan Y.H., Khalid M., Karri R.R., Walvekar R., Abdullah E.C., Nizamuddin S., Mazari S.A., 2021. A comprehensive review on magnetic carbon nanotubes and carbon nanotube-based buckypaper-heavy metal and dyes removal. Journal of Hazardous Materials. 125375.

13. Rastogi M., Nandal M., 2020. Toxic metals in industrial wastewaters and phytoremediation using aquatic macrophytes for environmental pollution control: an eco-remedial approach, In Bioremediation of Industrial Waste for Environmental Safety. Springer, 257-282.

14. Attar T., 2020. A mini-review on importance and role of trace elements in the human organism. Chem Rev Lett. 3(3), 117-130.

15. Briffa J., Sinagra E., Blundell R., 2020. Heavy metal pollution in the environment and their toxicological effects on humans. Heliyon. 6(9), e04691.

16. Genchi G., Carocci A., Lauria G., Sinicropi M.S., Catalano A., 2020. Nickel: Human health and environmental toxicology. International Journal of Environmental Research and Public Health. 17(3), 679.

17. Eskander S.B., Saleh H.M., 2020. Heavy Metal-Induced Oxidative Stress and Related Cellular Process. In Cellular and Molecular Phytotoxicity of Heavy Metals. Springer. 99-123.

18. Kapoor D., Singh M.P., 2021. Heavy metal contamination in water and its possible sources. In Heavy Metals in the Environment. Elsevier, 179-189.

19. Paithankar J.G., Saini S., Dwivedi S., Sharma A., Chowdhuri D.K., 2021. Heavy metal associated health hazards: An interplay of oxidative stress and signal transduction. Chemosphere. 262, 128350.

20. Li X., Shen S., Xu Y., Guo T., Dai H., Lu, X., 2021. Application of membrane separation processes in phosphorus recovery: A review. Science of the Total Environment. 767, 144346.

21. Qasem N.A., Mohammed R.H., Lawal D.U., 2021. Removal of heavy metal ions from wastewater: A comprehensive and critical review. Npj Clean Water. 4(1), 1-15.

22. Shindhal T., Rakholiya P., Varjani S., Pandey A., Ngo H.H., Guo W.Ng. H.Y., Taherzadeh M.J., 2021. A critical review on advances in the practices and perspectives for the treatment of dye industry wastewater. Bioengineered. 12(1), 70-87.

23. Chai W.S., Cheun J.Y., Kumar P.S., Mubashir M., Majeed Z., Banat F., Ho S.H., Show P.L., 2021. A review on conventional and novel materials towards heavy metal adsorption in wastewater treatment application. Journal of Cleaner Production. 126589.

24. Chua S.F., Nouri A., Ang W.L., Mahmoudi E., Mohammad A.W., Benamor A., Ba-Abbad M., 2021. The emergence of multifunctional adsorbents and their role in environmental remediation. Journal of Environmental Chemical Engineering. 9(1), 104793.

25. Singh S., Anil A.G., Kumar V., Kapoor D., Subramanian S., Singh J., Ramamurthy P.C., 2021. Nitrates in the environment: A critical review of their distribution, sensing techniques, ecological effects and remediation. Chemosphere. 131996.

26. Guidi P., Bernardeschi M., Palumbo M., Genovese M., Scarcelli V., Fiorati A., Riva L., Punta C., Corsi I., Frenzilli G., 2020. Suitability of a cellulose-based nanomaterial for the remediation of heavy metal contaminated freshwaters: A case-study showing the recovery of cadmium induced dna integrity loss, cell proliferation increase, nuclear morphology and chromosomal alterations on Dreissena polymorpha. Nanomaterials. 10(9), 1837.

27. Yadav M., Gupta R., Arora G., Yadav P., Srivastava A., Sharma R.K., 2020. Current Status of Heavy Metal Contaminants and Their Removal/Recovery Techniques. In Contaminants in Our Water: Identification and Remediation Methods. ACS Publications. 41-64.

28. Yuvaraj A., Thangaraj R., Karmegam N., Ravindran B., Chang S.W., Awasthi M.K., Kannan S., 2021. Activation of biochar through exoenzymes prompted by earthworms for vermibiochar production: A viable resource recovery option for heavy metal contaminated soils and water. Chemosphere. 130458.

29. Heidari-Maleni A., Gundoshmian T.M., Karimi B., Jahanbakhshi A., Ghobadian B., 2020. A novel fuel based on biocompatible nanoparticles and ethanol-biodiesel blends to

improve diesel engines performance and reduce exhaust emissions. Fuel. 276, 118079.

30. Jose L.M., Kuriakose S., Thomas S., 2020. Fabrication, Characterization and In Vitro Antifungal Property Evaluation of Biocompatible Lignin-Stabilized Zinc Oxide Nanoparticles Against Selected Pathogenic Fungal Strains. BioNanoScience. 10(3), 583-596.

31. Vandana U., Nancy D., Sabareeswaran A., Remya N., Rajendran, N., Mohanan P., 2021. Biocompatibility of strontium incorporated ceramic coated titanium oxide implant indented for orthopaedic applications. Materials Science and Engineering: B. 264, 114954.

32. Ratshiedana R., Kuvarega A.T., Mishra A.K., 2021. Titanium dioxide and graphitic carbon nitride–based nanocomposites and nanofibres for the degradation of organic pollutants in water: a review. Environmental Science and Pollution Research. 1-18.

33. Reddy P.V.G., Reddy B.R.P., Reddy M.V.K., Reddy K.R., Shetti N.P., Saleh T.A., Aminabhavi T.M., 2021. A review on multicomponent reactions catalysed by zero-dimensional/one-dimensional titanium dioxide (TiO_2) nanomaterials: Promising green methodologies in organic chemistry. Journal of Environmental Management. 279, 111603.

34. Tetteh E.K., Rathilal S., Asante-Sackey D., Chollom M.N., 2021. Prospects of Synthesized Magnetic TiO2-Based Membranes for Wastewater Treatment: A Review. Materials. 14(13), 3524.

35. Han T., Zhou D., Wang H., Zheng, X., 2015. The study on preparation and photocatalytic activities of Cu2O/TiO2 nanoparticles. Journal of Environmental Chemical Engineering. 3(4), 2453-2462.

36. Khairy M., Zakaria W., 2014. Effect of metal-doping of TiO_2 nanoparticles on their photocatalytic activities toward removal of organic dyes. Egyptian Journal of Petroleum. 23(4), 419-426.

37. Durante O., Di Giorgio C., Granata V., Neilson J., Fittipaldi R., Vecchione A., Carapella G., Chiadini F., DeSalvo R., Dinelli F., 2021. Emergence and Evolution of Crystallization in TiO_2 Thin Films: A Structural and Morphological Study. Nanomaterials. 11(6), 1409.

38. Wang J., Yin Z., Hermerschmidt F., List Kratochvil E.J., Pinna N., 2021. Impact of different intermediate layers on the morphology and crystallinity of TiO2 grown on carbon nanotubes by atomic layer deposition. Advanced Materials Interfaces. 8(15), 2100759.

39. Rezaei-Aghdam E., Shamel A., Khodadadi-Moghaddam M., Rajaei G.E., Mohajeri S., 2021. Synthesis of TiO_2 and ZnO Nanoparticles and CTAB-Stabilized Fe_3O_4 nanocomposite: kinetics and thermodynamics of adsorption. Research on Chemical Intermediates. 47(5), 1759-1774.

40. Bellahsen N., Varga G., Halyag N., Kertész S., Tombácz E., Hodúr C., 2021 Pomegranate peel as a new low-cost adsorbent for ammonium removal. International Journal of Environmental Science and Technology. 18(3), 711-722.

41. de Almeida G.C., Mohallem N.D.S., Viana M.M., 2021. Ag/GO/TiO_2 nanocomposites: the role of the interfacial charge transfer for application in photocatalysis. Nanotechnology. 33(3), 035710.

42. Mouchou R., Ukoba K., Laseinde O., Jen T., 2021. Fabrication of p-NiO/n-TiO_2 Solar Device for Photovoltaic Application. International Journal of Photoenergy. 2021.

43. Kusova A. M., Sitnitsky A.E., Zuev Y.F., 2021. The Role of pH and Ionic Strength in the Attraction–Repulsion Balance of Fibrinogen Interactions. Langmuir. 37(34), 10394-10401.

44. Ebrahimzadeh Rajaei G., Vojood A., 2019. Investigation of the Specific Ion Interactions and Determining Protonation Constant of 3, 5-Dihydroxy-2-(3, 4, 5-trihydroxybenzoyl) oxy-6-[(3, 4, 5-trihydroxybenzoyl) oxymethyl] oxan-4-yl] 3, 4, 5-trihydroxybenzoate at Different Ionic Strength. Iranian Journal of Chemistry and Chemical Engineering (IJCCE). 38(5), 91-98.

45. Arjaghi S.K., Alasl M.K., Sajjadi N., Fataei E., Rajaei G.E., 2021. Green Synthesis of Iron Oxide Nanoparticles by RS Lichen Extract and its Application in Removing Heavy Metals of Lead and Cadmium. Biological Trace Element Research. 199(2), 763-768.

46. Wang Q., Fang X., Hao P., Chi W., Huang F., Shi X., Cui G., Liu Y., Tang B., 2021. Green preparation of porous hierarchical TiO_2 (B)/anatase phase junction for effective photocatalytic degradation of antibiotics. Chemical Communications. 57, 13024-13027.

47. Rezaei-Aghdam E., Shamel A., Khodadadi-Moghaddam M., Ebrahimzadeh Rajaei G., Mohajeri, S., 2021. Hydrothermal synthesis of ZnO nanoparticles and comparison of its adsorption characteristics with the natural adsorbent (mango peel). Asian Journal of Nanosciences and Materials. 4(3), 188-200.

48. Müller F., Sauer J., Song X., Asmis K.R., 2021. The Chemical Nature of Ti_4O_{10}–: Vibrational Predissociation

Spectroscopy Combined with Global Structure Optimization. The Journal of Physical Chemistry A. 125(44), 9571–9577.

49. Nourzadeh Z., Anarjan N., Rajaei G.E., Jafarizadeh-Malmiri H., 2021. Preparation and characterization of vitamin D microemulsions using two-component surface-active stabilizer system, Zeitschrift für Physikalische Chemie. In press.

50. Vojood A., Khodadadi-Moghaddam M., Ebrahimzadeh-Rajaei G., Mohajeri S., Shamel A., 2021. Increasing in the Selectivity of Formose Reaction for Glyceraldehyde Production in the Presence of Fumed Silica and Montmorillonite Catalysts. Chemical Methodologies. 5(5), 422-432.

51. Zhang X., Wang X., 2015. Adsorption and desorption of nickel (II) ions from aqueous solution by a lignocellulose/montmorillonite nanocomposite. PloS One. 10(2), e0117077.

52. Le A.T., Pung S.Y., Sreekantan S., Matsuda A., 2019. Mechanisms of removal of heavy metal ions by ZnO particles. Heliyon. 5(4), e01440.

53. Rajaei G.E., Aghaie H., Zare K., Aghaie M., 2013. Adsorption of Cu (II) and Zn (II) ions from aqueous solutions onto fine powder of Typha latifolia L. root: kinetics and isotherm studies. Research on Chemical Intermediates. 39(8), 3579-3594.

54. Rajaei G.E., Khalili-Arjaghi S., Fataei E., Sajjadi N., Kashefi-Alasl M., 2020. Fabrication and characterization of polymer-based nanocomposite membrane modified by magnetite nanoparticles for Cd^{2+} and Pb^{2+} removal from aqueous solutions. Comptes Rendus. Chimie. 23(9-10), 563-574.

55. Kaur R., Singh J., Khare R., Cameotra S.S., Ali A., 2013. Batch sorption dynamics, kinetics and equilibrium studies of Cr (VI), Ni (II) and Cu (II) from aqueous phase using agricultural residues. Applied Water Science. 3(1), 207-218.